Current Biology 23, 1969–1978, October 21, 2013 http://dx.doi.org/10.1016/j.cub.2013.08.006

Article

An Atypical Tubulin Kinase Mediates Stress-Induced Microtubule Depolymerization in *Arabidopsis*

Satoshi Fujita,[1] Jaromir Pytela,[1] Takashi Hotta,[1] Takehide Kato,[1] Takahiro Hamada,[1] Rie Akamatsu,[1] Yasumasa Ishida,[1] Natsumaro Kutsuna,[2] Seiichiro Hasezawa,[2] Yuko Nomura,[3] Hirofumi Nakagami,[3] and Takashi Hashimoto[1,*]

[1]Graduate School of Biological Sciences, Nara Institute of Science and Technology, Ikoma, Nara 630-0192, Japan

[2]Department of Integrated Biosciences, Graduate School of Frontier Sciences, University of Tokyo, 5-1-5 Kashiwanoha, Kashiwa, Chiba 277-8562, Japan

[3]RIKEN Center for Sustainable Resource Science, Tsurumi-ku, Yokohama, Kanagawa 230-0045, Japan

Summary

Background: As sessile organisms, plants adapt to adverse environmental conditions by quickly adjusting cell physiology and metabolism. Transient depolymerization of interphase microtubules is triggered by various acute stresses and biotic interactions with pathogenic organisms. Although rapid remodeling of plant microtubule arrays in response to external stresses is an intriguing phenomenon, the underlying molecular mechanisms and the advantages of this response to plant performance are poorly understood.

Results: A domain with weak homology to the slime mold actin-fragmin kinase in the *Arabidopsis* mitogen-activated protein kinase phosphatase PROPYZAMIDE-HYPERSENSITIVE 1 (PHS1) is a Mn^{2+}-dependent kinase. This atypical kinase domain phosphorylates Thr349 of α-tubulin at the longitudinal interdimer interface, thereby generating a polymerization-incompetent isoform, and effectively depolymerizes microtubule arrays when ectopically expressed in plant or animal cells. The intrinsic tubulin kinase activity is normally suppressed by the phosphatase activity of PHS1 but is unmasked immediately after osmotic stress. In the *phs1* null mutant, stress-induced microtubule depolymerization does not occur.

Conclusions: The rapid and reversible modification of tubulin subunits by PHS1-mediated phosphorylation enables dynamic remodeling of the plant microtubule cytoskeleton in response to external stimuli. Suppression of the potent tubulin kinase activity by the juxtaposed phosphatase domain tightly controls this stress-activated microtubule regulator.

Introduction

Microtubules are protein filaments that assemble from α/β-tubulin heterodimers and form dynamic cytoskeletal networks that support a wide variety of cellular processes. During mitosis, the mitotic spindle serves as a highly dynamic scaffold used to precisely segregate chromosomes to daughter cells, whereas plant-specific microtubule structures, such as preprophase bands and phragmoplasts, execute developmentally determined positioning of a new cell plate between two daughter cells [1]. In the interphase, microtubule networks adopt various configurations, from radial to linear [2]. Cortical microtubule arrays in the interphase plant cell spread in a quasi-2D sheet in association with the inner face of the plasma membrane. These cortical arrays guide the movement of cellulose-synthase complexes, thereby contributing to the cell's directional expansion and shape [3].

Apart from these well-known roles of plant microtubules in cell division and cell morphology, it has been frequently documented that environmental signals affect the organization of microtubule networks, possibly contributing to plant adaptation in response to changing environments. The cortical arrays change during tropic responses to light and gravity and after the application of plant hormones, and disassemble in response to low temperature and aluminum or salt stress [4–7]. During biotic interactions with nematodes and phytopathogenic bacteria and fungi, cortical microtubules are extensively reorganized and, in some cases, transiently depolymerized [8]. In addition to the interphase arrays, cold-induced destabilization of postmeiotic microtubule arrays generates diploid male gametes, possibly contributing to plant polyploidization and associated speciation [9]. Although these changes in microtubule stability and organization may involve alterations in microtubule stability and dynamics, intermicrotubule association, microtubule nucleation activity, and interactions with the plasma membrane and other cellular components, the underlying molecular mechanisms remain largely elusive.

A semidominant mutant of *Arabidopsis thaliana*, *propyzamide-hypersensitive 1-1d* (*phs1-1d*), which has partially destabilized cortical microtubules and shows left-handed helical growth, is caused by an Arg64-to-Cys (R64C) missense mutation in the putative kinase-interacting motif (KIM) of a mitogen-activated protein kinase (MAPK) phosphatase [10], whereas null mutant alleles of *PHS1* are indistinguishable from the wild-type (WT) under standard growth conditions [11]. PHS1 is predominantly cytoplasmic [11] and interacts with and in vitro dephosphorylates MAPK18 [12], which belongs to the D group MAPKs consisting of eight members in *Arabidopsis* [13]. It has been unknown how the semidominant R64C mutation of PHS1 evokes partial microtubule destabilization, and what developmental or environmental signals activate the PHS1's microtubule-destabilizing function. In this work, we show that PHS1 possesses an atypical kinase domain in addition to the MAPK phosphatase domain. The kinase domain phosphorylates α-tubulin to generate a polymerization-incompetent form, thereby efficiently destabilizing microtubules. Moreover, the phosphatase activity in PHS1 normally suppresses the tubulin kinase activity in planta, but a hyperosmotic stress relieves the phosphatase inhibition and potentiates the tubulin phosphorylation activity.

Results

Phosphatase-Dead PHS1 Mutation Causes Depolymerization of Cortical Microtubules in *Arabidopsis* Plants

The R64C mutation in the putative KIM of PHS1 might decrease an interaction between PHS1 and its putative target,

*Correspondence: hasimoto@bs.naist.jp

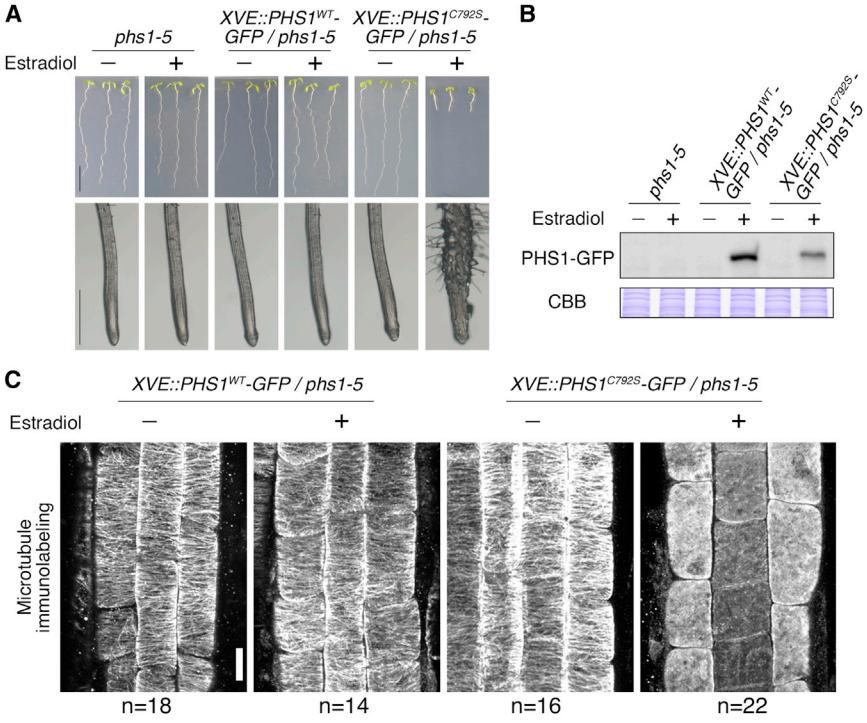

Figure 1. Expression of Phosphatase-Dead PHS1 Causes Radial Cell Expansion and Microtubule Depolymerization

(A) *Arabidopsis phs1-5* null mutant seedlings and those transformed with an estradiol-inducible *PHS1-GFP* gene were grown in the absence (–) or presence (+) of 5 μM estradiol for 7 days. Wild-type (WT) or a phosphatase-dead C792S mutant of PHS1 was expressed. Scale bars represent 1 cm (whole seedlings) and 500 μm (primary roots).

(B) Protein extracts of *Arabidopsis* seedlings grown in the absence (–) or presence (+) of 5 μM estradiol for 24 hr were analyzed by immunoblotting with anti-PHS1 antibody. CBB-stained images are shown as loading controls.

(C) Four-day-old transgenic *Arabidopsis* seedlings were incubated for 6 hr in the medium containing 0.05% DMSO (–) or 5 μM estradiol (+), and microtubules were visualized by immunostaining with anti-α-tubulin antibody. Representative images of cortical microtubules in root epidermis cells at the early elongation zones are shown as stacks of confocal sections. "n" indicates the total number of observed roots. Scale bar represents 10 μm.

See also Figure S1.

such as MAPK18, and might reduce the phosphatase activity against the target substrate. To explore this possibility further, we examined whether a phosphatase-dead form of PHS1 acts as a dominant-negative microtubule destabilizer in planta. We first expressed a GFP fusion of WT PHS1 (PHS1-GFP) upon estradiol induction in the *phs1-5* null allele background and found that growth and morphology of the stably transformed *Arabidopsis* plants were indistinguishable from WT and *phs1-5*. When a GFP fusion of the phosphatase-dead Cys792-to-Ser mutant (PHS1^{C792S}-GFP) [10] was inducibly expressed in *phs1-5*, however, *Arabidopsis* seedlings were severely dwarfed, and root epidermal cells at the elongation and differentiation zones were radially expanded (Figure 1A). Immunoblot analysis with an anti-PHS1 antibody showed that full-length PHS1-GFP and PHS1^{C792S}-GFP were expressed after estradiol treatment (Figure 1B). The cortical microtubules in root epidermal cells (as immunostained by a tubulin antibody) were well organized into transverse arrays in PHS1-GFP-expressing plants but almost completely depolymerized in plants expressing PHS1^{C792S}-GFP after estradiol induction (Figure 1C).

We also expressed genomic fragments of *PHS1* as GFP fusions in transgenic *Arabidopsis* plants (see Figure S1A available online). The WT *PHS1* transgene (gPHS1^{WT}-GFP) did not produce any phenotypes, whereas the R64C mutant (gPHS1^{R64C}-GFP) reproduced the *phs1-1d* left-handed helical growth phenotypes. The phosphatase-dead C792S mutant in combination with R64C (gPHS1$^{R64C, C792S}$-GFP) yielded severe dwarf plants with radially expanded cells. Cortical microtubules in root epidermal cells were well organized in transverse arrays in gPHS1^{WT}-GFP, partially compromised in gPHS1^{R64C}-GFP, and substantially depolymerized in gPHS1$^{R64C, C792S}$-GFP (Figure S1B). Immunoblot analyses with GFP and PHS1 antibodies showed that PHS1^{WT}-GFP and PHS1^{R64C}-GFP were more abundant than endogenous PHS1 and migrated as doublets on the SDS-PAGE gel, whereas PHS1$^{R64C, C792S}$-GFP was less abundant than endogenous PHS1 and present as a slowly migrating singlet band (Figure S1C). These results show that the phosphatase-inactive form of PHS1 induces cortical microtubule destabilization in *Arabidopsis* cells.

A Central Domain Excluding the Phosphatase Domain Depolymerizes Microtubules In Vivo

A phosphatase-dead form of PHS1 might somehow act to interfere and poison a cellular signaling pathway leading to microtubule destabilization. Alternatively, PHS1 might possess an intrinsic microtubule-destabilizing activity, which is normally suppressed by its phosphatase activity. To characterize the domain structure of PHS1 with regard to its potential microtubule-destabilizing activity, we set up a transient expression assay in which a mutant PHS1 protein was transiently expressed by particle bombardment into *Arabidopsis* leaf epidermal cells where cortical microtubules were labeled by stable expression of GFP-β-tubulin (GFP-TUB; [14]) (Figures 2A and 2B). A plasmid encoding a red fluorescent protein (mCherry) was simultaneously introduced to locate the transformed cells. Cortical microtubules were depolymerized in PHS1^{C792S}-expressing cells, but not in cells expressing WT PHS1. Phosphatase-dead mutations of the corresponding catalytic Cys in four other *Arabidopsis* MAPK phosphatases did not produce microtubule-destabilizing effects, indicating specificity of the PHS1 phosphatase (Figure S2A). The R64C substitution in the putative KIM weakly destabilized cortical microtubules (Figure 2A). After testing various truncations of PHS1, we found that an internal 69 kDa fragment (aa 85–700) that lacked the phosphatase catalytic domain and the putative KIM (PHS1ΔP) is necessary and sufficient for the microtubule-destabilizing activity (Figures 2A and 2B). The catalytically active phosphatase domain (but not its inactive form) suppressed the microtubule-depolymerizing effect of PHS1ΔP when supplied in *trans* by a different plasmid (Figure 2C). Actin

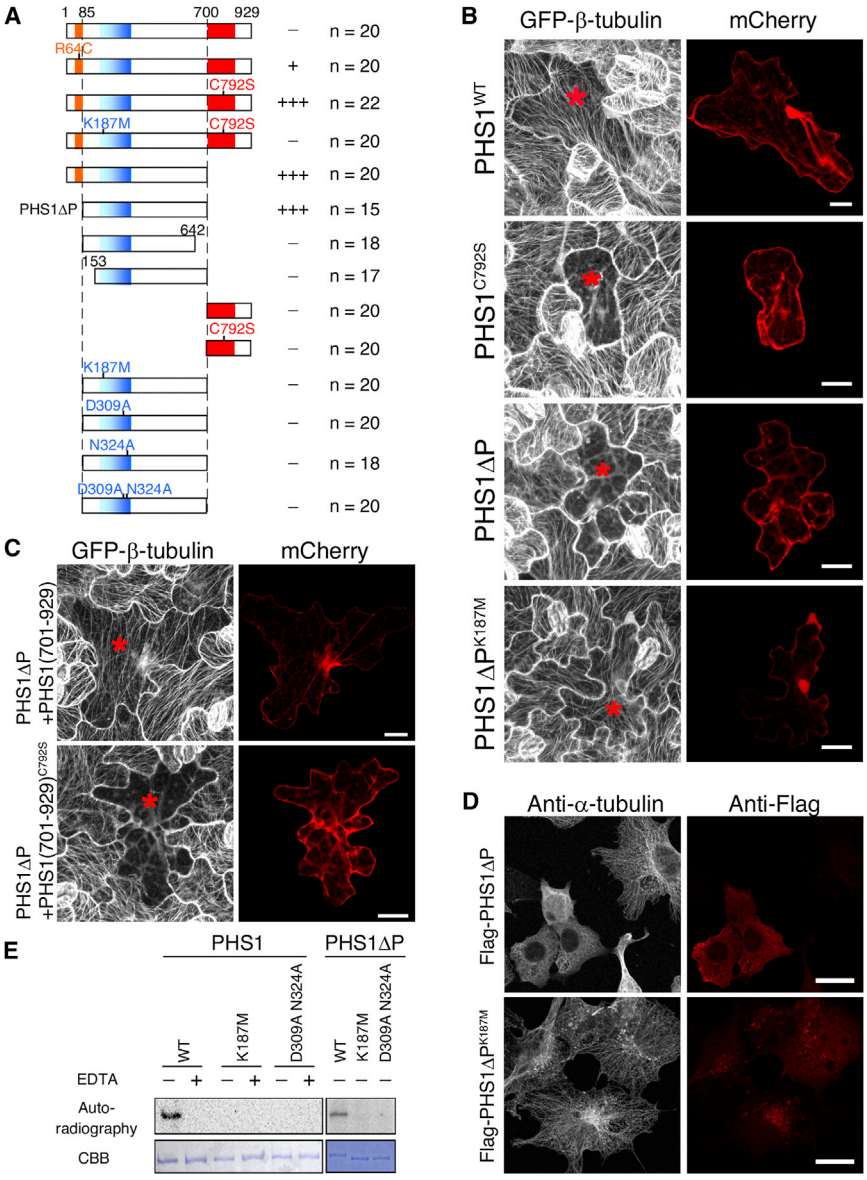

Figure 2. An Atypical Kinase Domain in PHS1 Destabilizes Microtubules In Vivo

(A) Summary of transient expression assays. Full-length, truncated, or mutated PHS1 forms were transiently expressed with the mCherry transformation marker in *Arabidopsis* leaf epidermis cells expressing GFP-β-tubulin. –, intact microtubules; +, microtubules partially destabilized but still present; +++, microtubules totally depolymerized. "n" indicates the total number of observed cells for each construct. The putative kinase-interacting motif (KIM; orange), a homology region to actin-fragmin kinase (blue), the MAPK phosphatase domain (red), and mutated amino acid residues are indicated.

(B) Expression of PHS1ΔP and phosphatase-dead PHS1 destabilized cortical microtubules in *Arabidopsis* leaf pavement cells. Successfully transformed cells were identified by the red fluorescence of mCherry (right) and are indicated in red asterisks (left). Scale bars represent 20 μm.

(C) The active phosphatase domain suppresses the microtubule depolymerization activity of PHS1ΔP when supplied in *trans*. PHS1ΔP and the phosphatase domain (aa 701–929) were expressed from different plasmids, together with mCherry. Fifteen transformed cells were analyzed per each combination. Red asterisks mark transformed cells. Scale bars represent 20 μm.

(D) PHS1ΔP strongly depolymerizes interphase microtubules in COS-7 cells. Flag-tagged PHS1ΔP or its kinase-dead form (PHS1ΔP ^{K187M}) was expressed. Microtubules were stained with α-tubulin antibody (left), while transformed cells were located by immunostaining with Flag antibody (right). For each construct, 40 transformed cells were analyzed. Scale bars represent 20 μm.

(E) Recombinant full-length PHS1 and its kinase domain (PHS1ΔP) show a Mn^{2+}-dependent autophosphorylation activity in the presence of radioactive ATP. Mutation of the catalytic Lys187 residue or chelation of Mn^{2+} with EDTA abolished the autophosphorylation activity. Proteins were stained with Coomassie brilliant blue (CBB).

See also Figure S2.

filaments were not depolymerized by ectopically expressed WT or phosphatase-inactive PHS1 (Figure S2B). Interestingly, expression of PHS1ΔP effectively depolymerized interphase microtubules in cultured COS-7 monkey cells (Figure 2D). We thus conclude that PHS1 potentially depolymerizes microtubules of plant and mammalian origins, but this activity is normally suppressed by the phosphatase activity endowed in the same protein.

Microtubule-Destabilizing Activity Resides in an Autophosphorylating Kinase Domain with Homology to Actin-Fragmin Kinase

PHS1ΔP contains a low level of amino acid sequence similarity to the atypical kinase domain of slime mold actin-fragmin kinase (Figures S2C and S2D), which phosphorylates Thr202 and Thr203 in the actin subunit of the actin-fragmin complex [15, 16]. Lys187, Asp309, and Asn324 (numbered according to *Arabidopsis* PHS1) are conserved among actin-fragmin kinase and putative plant PHS1 orthologs (Figures S2D and S2E) and interact with the bound nucleotide in actin-fragmin kinase [17]. Mutation of these residues indeed inactivated PHS1ΔP-containing fragments in the transient microtubule-depolymerization assays in *Arabidopsis* and monkey cells (Figures 2A, 2B, and 2D). To examine whether the actin-fragmin kinase homology region has basal kinase activity, we purified WT PHS1 and two PHS1 mutants (as fusions to the Trigger Factor) from *E. coli* and assayed their autophosphorylation activities (Figure 2E). Both full-length and ΔP forms of WT PHS1 underwent autophosphorylation in the presence of ATP and Mn^{2+}, whereas the Lys187-to-Met single mutation and the Asp309-to-Ala, Asn324-to-Ala double mutations both abolished the autophosphorylation activity. Chelation of Mn^{2+} with EDTA completely inhibited the kinase activity, indicating a requirement of this cation. Full-length recombinant PHS1 showed basal kinase activity in vitro, despite being inactive on cortical microtubules in vivo (Figure 2E). Thus, PHS1 possesses an atypical kinase domain juxtaposed with an MAPK phosphatase domain.

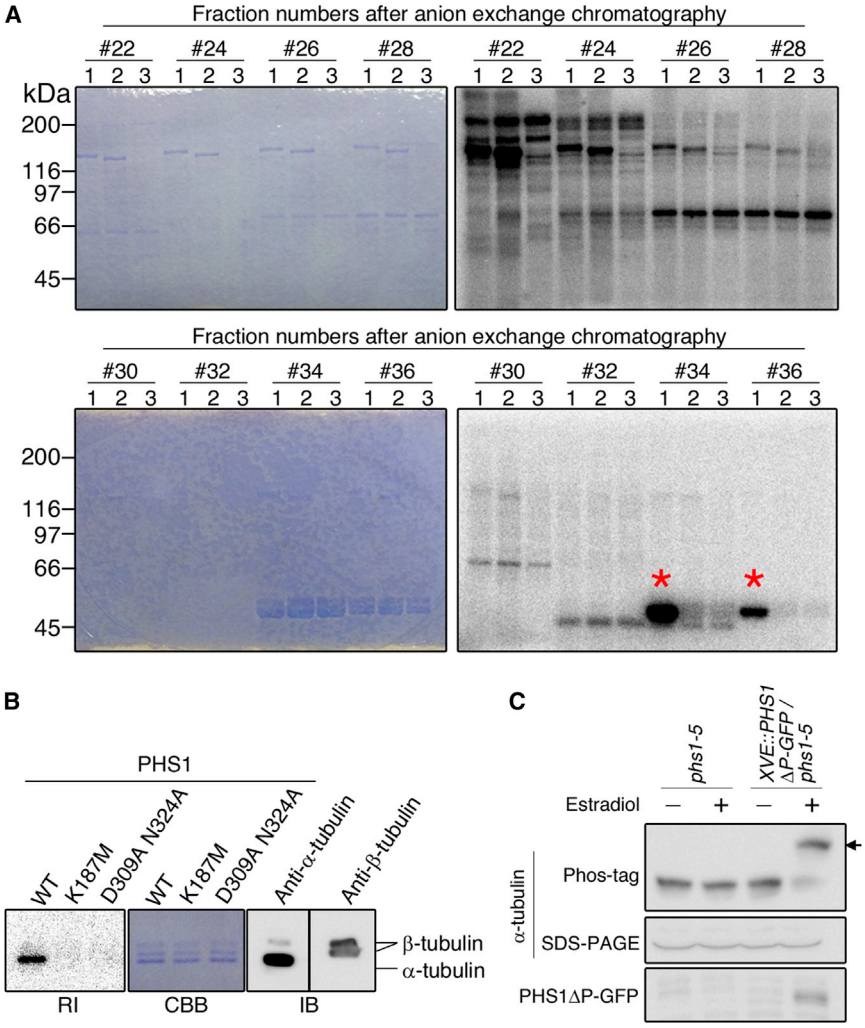

Figure 3. PHS1 Phosphorylates α-Tubulin In Vivo and In Vitro

(A) In vitro screening of PHS1 substrates. *Arabidopsis* microtubule-associated proteins and tubulins were fractionated by anion exchange column chromatography, and each fraction was subjected to a kinase assay in vitro with recombinant TF-Strep-tagged PHS1ΔP (lane 1), catalytically inactive TF-Strep-tagged PHS1ΔP $^{D309A,\ N324A}$ (lane 2), or buffer (lane 3) in the presence of [γ-^{32}P]ATP. Proteins specifically phosphorylated by PHS1ΔP (red asterisks) were detected in fractions 34 and 36. Coomassie brilliant blue-stained proteins (left panels) and autoradiography images (right panels) are shown.

(B) PHS1 phosphorylates α-tubulin in vitro. *Arabidopsis* α- and β-tubulins were separated by SDS-PAGE and detected by immunoblotting. α-tubulin antibody mostly detected the 48.5 kDa band and faintly detected the 52 kDa band, whereas β-tubulin antibody recognized the 50 and 52 kDa bands. WT PHS1 phosphorylated α-tubulin in vitro, but a kinase-dead PHS1^{K187M} mutant did not. The autoradiography image (RI) and the CBB-stained image were obtained from the same gel, whereas immunoblots (IB) were from a similarly processed different gel.

(C) PHS1ΔP phosphorylates α-tubulin in vivo. Expression of the kinase domain (PHS1ΔP-GFP) was induced by estradiol (+) in XVE::PHS1ΔP-GFP/*phs1-5* plants. Immunoblot analysis of α-tubulin after Phos-tag SDS-PAGE revealed a phosphorylated α-tubulin isoform (arrow) upon the in vivo expression of PHS1ΔP-GFP.

See also Figure S3.

PHS1 Phosphorylates α-Tubulin

To identify physiological substrates of PHS1, we tested whether *Arabidopsis* cytosolic proteins enriched for microtubule-associated proteins could be phosphorylated by active PHS1ΔP. After fractionation with anion exchange chromatography, soluble proteins in individual eluted fractions were subjected to an in vitro kinase reaction with PHS1ΔP, PHS1ΔP$^{D309A,\ N324A}$, or buffer. Reaction products were then separated on SDS-PAGE and analyzed by protein staining and autoradiography (Figure 3A). Acidic proteins of ~50 kDa in the fractions 34 and 36, corresponding to tubulins, were efficiently phosphorylated by active PHS1ΔP, but not by inactive PHS1ΔP$^{D309A,\ N324A}$. No other proteins in the preparations showed differential phosphorylation between PHS1ΔP and PHS1ΔP$^{D309A,\ N324A}$. When tubulins were purified from *Arabidopsis* cultured cells and analyzed after the in vitro kinase reaction under a SDS-PAGE condition that separated α- and β-tubulins, α-tubulin, but not β-tubulin, was phosphorylated by PHS1ΔP, but not by the kinase-dead mutants PHS1ΔP^{K187M} and PHS1ΔP$^{D309A,\ N324A}$ (Figure 3B). Pig tubulins were also phosphorylated by active PHS1, but heat-denatured tubulins (either of *Arabidopsis* or pig origin) were not (Figure S3), indicating that the native tubulin structure is required for the phosphorylation.

We next expressed an estradiol-inducible form of WT PHS1ΔP-GFP in *phs1-5* and analyzed α-tubulin by immunoblots using an α-tubulin antibody (Figure 3C). Migration of phosphorylated proteins is expected to be retarded on a Phos-tag gel [18]. We detected a slowly migrating band of α-tubulin when PHS1ΔP-GFP expression was induced by estradiol, but not in control samples. These results show that a major in vivo substrate of the PHS1 kinase is α-tubulin.

Threonine 349 of α-Tubulin Is Phosphorylated by PHS1

To identify the phosphorylated amino acid residue (or residues) of α-tubulin, active PHS1ΔP-GFP was immunoprecipitated by a GFP antibody from the estradiol-induced *Arabidopsis* plants (see Figure 3C) and used to phosphorylate purified tubulins. We used pig tubulins as substrates because no endogenous phosphorylations were detected in this sample during our preliminary experiments. Figure 4A shows SDS-PAGE analysis of the in vitro kinase reaction products after incubation with buffer (sample 1), immunoprecipitated proteins from *phs1-5* plants (sample 2), or immunoprecipitated proteins from PHS1ΔP-GFP-expressing *phs1-5* plants (sample 3). Mass spectrometry analysis revealed that a phosphopeptide of α-tubulin containing phosphorylated Thr349 was detected in sample 3, but not in samples 1 and 2, whereas the corresponding nonphosphorylated peptide was found in all samples (Figures 4B and 4C). Thr349 was the sole and specifically phosphorylated residue; no other PHS1-dependent modifications of α- and β-tubulins were observed (Figure 4D).

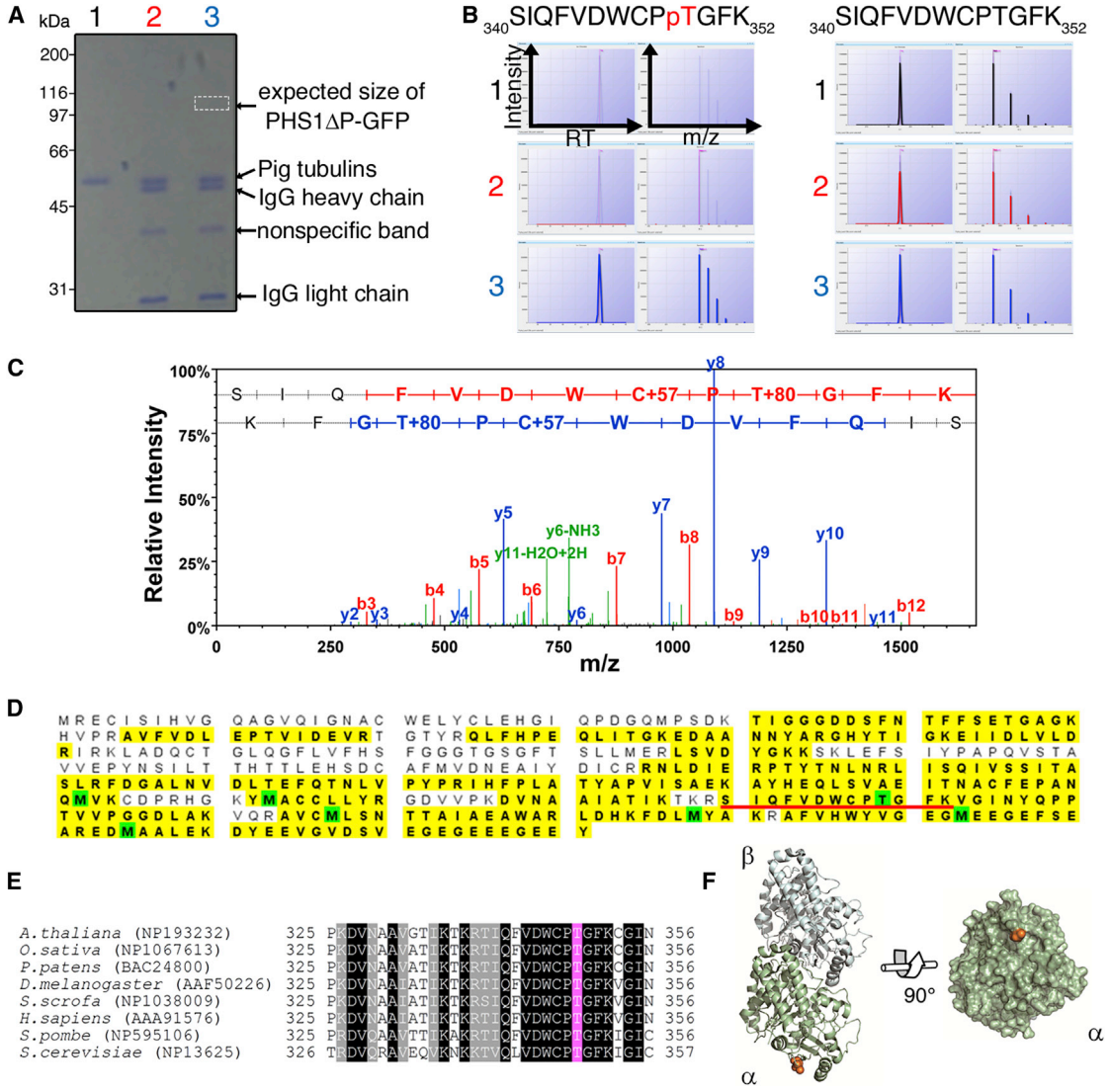

Figure 4. PHS1 Phosphorylates α-Tubulin at the Site of Thr349

(A) Samples for the MS analysis are shown. Pig tubulins were incubated without (sample 1) or with (samples 2 and 3) immunoprecipitates in the ATP-containing kinase assay buffer. Crude protein extracts from *Arabidopsis phs1-5* seedlings (sample 2) or transgenic *phs1-5* seedlings expressing PHS1ΔP-GFP after estradiol induction were treated with GFP antibody-coupled beads and immunoprecipitated. After the reaction, samples were subjected to SDS-PAGE and CBB staining. In lane 3, a very faint band corresponding to PHS1ΔP-GFP (dotted box) was visible after scrutiny.

(B) Chromatograms of selected ions representing two peptides (left) and mass ions of these peptides, showing a few higher-mass species due to the presence of stable isotopes (right). The phosphopeptide 340-SIQFVDWCPpTGFK-352 was detected only in sample 3, but not in samples 1 and 2, whereas the corresponding nonphosphorylated peptide was observed in all samples. RT, retention time.

(C) MS/MS spectrum of a phosphopeptide (340-SIQFVDWCPpTGFK-352) from PHS1-treated pig α-tubulin. Labeled peaks correspond to masses of b and y ions of the modified peptides.

(D) Amino acid sequence of *Sus scrofa* α-tubulin 1B. A total of 26 unique peptides (yellow) were identified and covered 66% of the sequence. PHS1-dependent modification was only identified at Thr349 in a peptide (underlined in red). Met residues (green) were oxidatively modified in all samples.

(E) Multiple amino acid sequence alignment of a region surrounding Thr349 (asterisk) from various α-tubulins. Accession numbers for each α-tubulin are indicated.

(F) α/β-tubulin heterodimer structures in a ribbon diagram (left) and a surface-filling model (right), which has been rotated 90° to the indicated direction. Thr349 is highlighted in orange.

Phosphorylation of Thr349 has been detected in *Arabidopsis* α-tubulins [19, 20]. This residue is highly conserved in α-tubulins from various organisms (Figure 4E) [20] and is located at the interdimer longitudinal contact site with β-tubulin in a microtubule protofilament (Figure 4F) [21]. Addition of a phosphate group to this Thr is expected to impair longitudinal interactions between two adjacent tubulin heterodimers in a protofilament. Because Thr349 phosphorylation of nonplant α-tubulins is not detected in phosphor proteome databases, such as Phospho.ELM (http://phospho.elm.eu.org/), PHOSIDA (http://www.phosida.com/), and PhosphoSitePlus (http://www.phosphosite.org/homeAction.do), the kinase activity targeting this Thr residue appears to be specifically present in plants.

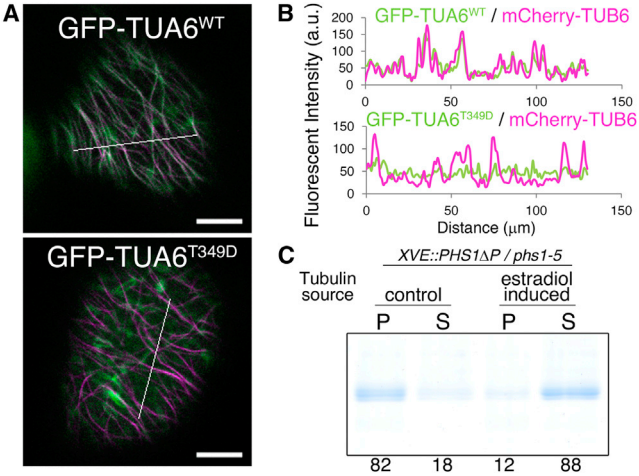

Figure 5. α-Tubulin Phosphorylated at Thr349 Does Not Assemble into Microtubules

(A) GFP-labeled WT α-tubulin (TUA6^{WT}) coassembled with mCherry-labeled β-tubulin (TUB6) in microtubule polymers, but a phosphomimic mutant (GFP-TUA6^{T349D}) was not incorporated into mCherry-labeled microtubules in *Arabidopsis* leaf pavement cells. Scale bars represent 10 μm.

(B) Intensity plots of GFP and mCherry signals along the white lines in (A).

(C) SDS-PAGE analysis of microtubule sedimentation assay using tubulins purified from XVE::PHS1ΔP-GFP/*phs1-5* plants before (control) and after induction of PHS1ΔP-GFP by estradiol as shown in Figure 4C. Distribution ratios of recovered tubulins between pellet (P) and supernatant (S) are indicated.

α-Tubulin Phosphorylated at Thr349 Is Not Incorporated into Microtubules

To test whether tubulins phosphorylated by PHS1 polymerize to microtubules in vivo, we coexpressed GFP-TUA6 (which labeled α-tubulin) and mCherry-TUB6 (which labeled β-tubulin) in transgenic *Arabidopsis* plants (Figures 5A and 5B). GFP and mCherry fluorescence overlapped in *Arabidopsis* lines stably expressing mCherry-TUB6 and GFP-labeled WT TUA6 (GFP-TUA6^{WT}), indicating that both fusion tubulin proteins were coassembled into microtubules. In contrast, GFP-TUA6^{T349D} (containing a phosphomimic mutation of the PHS1 target site) was scarcely incorporated into mCherry-TUB6-labeled microtubules. Pearson's correlation coefficients of the GFP and mCherry signal colocalization are 0.51 ± 0.10 (mean ± SD) for WT TUA (n = 15) and 0.18 ± 0.07 for the Thr349-to-Asp mutant (n = 13), significantly different from the WT value ($p < 0.001$; Mann-Whitney U test).

Next, we examined whether tubulins phosphorylated by PHS1 polymerize to microtubules in vitro. A recently developed TOG1/TOG2 tubulin affinity purification resin [22] was used to purify tubulins from *Arabidopsis* seedlings (XVE::PHS1ΔP-GFP/*phs1-5*) before or after induction of PHS1ΔP-GFP by estradiol. The microtubule sedimentation assay showed that tubulins purified from the control plants polymerized efficiently in the presence of 5 μM Taxol, but tubulins from PHS1ΔP-GFP-expressing plants scarcely assembled into microtubules in vitro (Figure 5C). Because we did not detect any PHS1-dependent tubulin modifications other than Thr349 phosphorylation of α-tubulin in vitro, and because the in vitro microtubule assembly experiment only involved purified tubulins, it is unlikely that PHS1ΔP has another inhibitory effect on tubulin assembly. These results strongly suggest that α-tubulin phosphorylated at Thr349 by PHS1 does not readily assemble to the microtubule polymer in vitro and in vivo.

Stress-Induced Microtubule Depolymerization Is Mediated by PHS1

Exposure of *Arabidopsis* seedlings to high concentrations of salt or osmolyte induces transient depolymerization of cortical microtubules in epidermal cells [5, 23, 24]. Thr349 of α-tubulin was recently implicated as the stress-induced phosphorylation site when various α-tubulin Thr mutations were expressed and analyzed in rice cells [24]. Therefore, we tested a possibility that PHS1 is involved in salt- or osmolyte-induced depolymerization of cortical microtubules in planta. High-salt stress (0.4 M NaCl) or hyperosmotic stress (0.8 M sorbitol) promoted the accumulation of phosphorylated α-tubulin (which was susceptible to a phosphatase treatment in vitro) in WT *Arabidopsis* plants, but not in *phs1-5* null mutant plants (Figures 6A and 6B). Tubulin phosphorylation occurred in WT dark-grown plants within 10 min of exposure to high osmotic conditions and decreased after 30 min (Figure 6C). α-tubulin mutated at the target residue of the PHS1 tubulin kinase (TUA6^{T349A}) was not phosphorylated under these conditions when expressed in *Arabidopsis* plants (Figure 6D), indicating that the slowly migrating α-tubulin isoform is phosphorylated at Thr349. Cortical microtubules in the etiolated hypocotyl epidermal cells of *phs1-5* were not depolymerized after high-sorbitol treatment, in contrast to those in WT cells (Figures 6E and S4), demonstrating that PHS1-dependent tubulin phosphorylation is responsible for the stress-induced microtubule depolymerization. Quantification of the microtubule polymer density showed that, consistent with the timing of tubulin phosphorylation, significant microtubule depolymerization occurred within 10 min of sorbitol treatment in WT, but not in *phs1-5* (Figure 6F).

Discussion

In this study, we showed that PHS1 is an autoregulated tubulin kinase. The active site of the kinase domain contains limited but significant homology, including three functionally critical amino acid residues involved in ATP binding, to the slime mold actin-fragmin kinase [17]. The tubulin kinase activity requires larger regions beyond the actin-fragmin kinase homology region, and these extended regions may be involved in recognition of native tubulins as in vivo substrates. Interestingly, animals and many fungi do not have proteins containing significant homology to the kinase domain found in PHS1 and actin-fragmin kinase. PHS1-mediated phosphoregulation of microtubule stability appears to be unique to the plant kingdom.

PHS1 is a hybrid microtubule regulator in which a tubulin kinase domain is embedded within the negatively acting MAPK phosphatase molecule. Because α-tubulin is not normally phosphorylated in *Arabidopsis* plants grown in standard growth conditions and full-length PHS1 does not affect microtubule stability when expressed transiently or stably in *Arabidopsis* cells, the tubulin kinase activity of PHS1 should be suppressed by the adjacent phosphatase in nonstressed plant cells. PHS1 interacts with *Arabidopsis* MAPK18 and dephosphorylates autophosphorylated recombinant MAPK18 in vitro [12], implying that MAPK18 and possibly other MAPKs may activate the tubulin kinase domain of PHS1, but that those MAPKs are normally inactivated by the phosphatase domain of PHS1 (Figure 6G). Salt and osmotic stresses may relieve

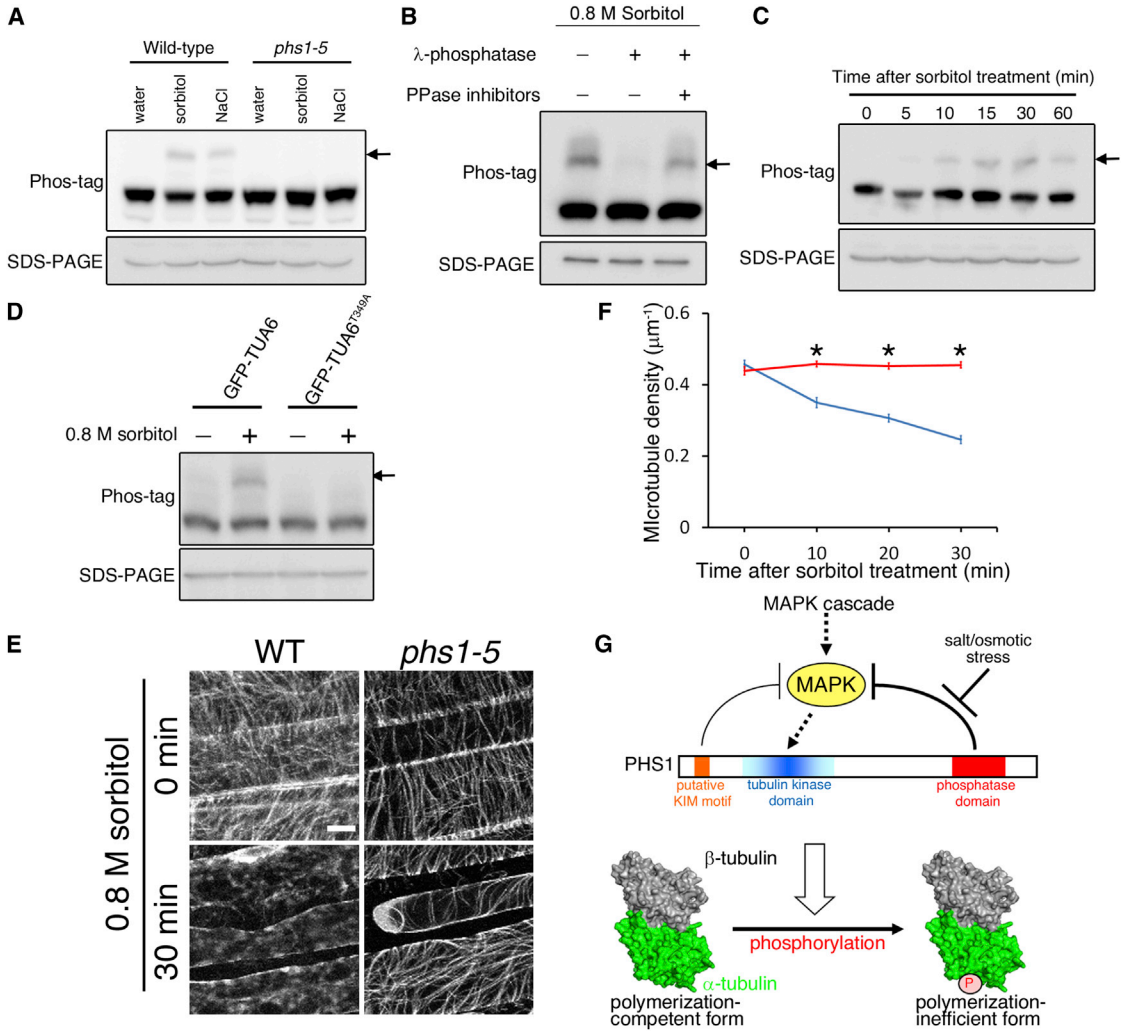

Figure 6. Osmotic Stress Induces Microtubule Depolymerization in *Arabidopsis* Plants by PHS1-Mediated α-Tubulin Phosphorylation

(A) PHS1-dependent accumulation of phosphorylated α-tubulin under stress. Treatment with 0.8 M sorbitol or 0.4 M NaCl for 1 hr caused phosphorylated α-tubulins (arrow) to accumulate in WT seedlings, but not in *phs1-5* seedlings. Immunoblot analysis detected α-tubulins after electrophoresis on Phos-tag and SDS-PAGE gels.

(B) A slowly migrating band on Phos-tag gel is phosphorylated α-tubulin. GFP-TUA6 was immunoprecipitated using anti-GFP antibody-coupled beads from *Arabidopsis* seedlings expressing GFP-TUA6^{WT}, which had been treated with 0.8 M sorbitol for 60 min, and was treated with λ-phosphatase in the absence (−) or presence (+) of protein phosphatase inhibitors. After incubation, proteins were separated on Phos-tag or SDS-PAGE gels and detected by anti-GFP antibody. An arrow indicates phosphorylated GFP-TUA6.

(C) Time course of phosphorylated α-tubulin accumulation (arrow) after treatment with 0.8 M sorbitol in the dark-grown hypocotyls.

(D) Thr349 of α-tubulin is phosphorylated by hyperosmotic stress. *Arabidopsis* seedlings expressing GFP-TUA6^{WT} or GFP-TUA6^{T349A} were treated with 0.8 M sorbitol for 60 min. Proteins were extracted from treated (+) and nontreated (−) plants, separated on Phos-tag or SDS-PAGE gels, and detected by anti-GFP antibody. GFP-TUA6^{T349A} was not phosphorylated. An arrow indicates phosphorylated GFP-TUA6.

(E) Cortical microtubule arrays labeled with GFP-TUB6 in the etiolated hypocotyl cells of WT seedlings and *phs1-5* seedlings before and after treatment with 0.8 M sorbitol for 30 min. Hyperosmotic stress induced plasmolysis in both cell types but caused microtubule depolymerization only in WT cells. Scale bar represents 10 μm.

(F) Microtubule density after sorbitol-induced plasmolysis. Microtubule density decreased within 10 min of sorbitol treatment in the WT (blue) but did not change in *phs1-5* (red). Values are means ± SEM (65 cells from seven WT seedlings, and 66 cells from ten *phs1-5* seedlings). Asterisks indicate statistically significant differences (Welch's t test, *p < 0.001).

(G) Activation model of the PHS1 tubulin kinase and subsequent Thr349 phosphorylation of α-tubulin to a polymerization-inefficient form.

See also Figure S4.

dephosphorylation-mediated MAPK inactivation, rather than activating upstream MAPK signaling, because a tubulin kinase domain lacking the inhibitory phosphatase is constitutively active even in the absence of the stimulating stress signals in vivo.

The phosphorylated Thr349 is highly conserved in many α-tubulin proteins from various eukaryotes, which likely serve as potential substrates of PHS1, as we demonstrated for microtubules in COS-7 cells and purified pig tubulins. A high-resolution model of the microtubule protofilament predicts that this Thr residue of α-tubulin longitudinally interacts with Val177 of β-tubulin in the adjacent tubulin heterodimer [21]. It has been reported that Thr349-to-Ile dominant mutations in *Arabidopsis* α-tubulin 2 (TUA2) and TUA4 cause

hypersensitivity to microtubule-depolymerizing drugs and strong left-handed helical growth in a dominant-negative manner [25], supporting the functional importance of Thr349 of α-tubulins in microtubule stability.

Tubulin heterodimers phosphorylated at Thr349 of α-tubulin did not polymerize in the presence of a low dose of Taxol in vitro, and the phosphomimic Thr349-to-Asp α-tubulin mutant did not assemble into the microtubule polymer in vivo. Similar results were reported for yeast phosphomimic Thr349-to-Glu α-tubulin mutant [26]. Because relatively low levels of the stress-induced phosphorylated α-tubulin, compared to nonphosphorylated forms, triggered depolymerization of cortical microtubules in *Arabidopsis* epidermal cells, we speculate that Thr349 phosphorylation of α-tubulin might inhibit microtubule polymerization dominant negatively. A polymerization-blocked yeast tubulin mutant was reported to inhibit the polymerization of WT tubulin when present in mixtures, thus acting as a dominant-negative polymerization inhibitor [26]. The molecular mechanism of this dominant-negative inhibition is not known, but the phosphorylated or phosphomimic tubulins might transiently or weakly associate with the GTP cap at the plus end, thereby destabilizing this structure. Further mechanistic analyses are required to understand the apparent dominant-negative effect of the tubulin modification.

Posttranslational modifications of tubulin subunits, such as detyrosination/tyrosination, acetylation, polyglutamylation, and polyglycylation, diversify the outer and luminal surfaces of distinct subpopulations of microtubules and potentially provide mechanisms that locally regulate microtubule-based activities in the same cell [27, 28]. Posttranslational modifications of plant tubulins and their consequences on microtubule functions are still poorly understood. *Arabidopsis* kinases belonging to the casein kinase family [29] and the NimA-related kinase family [30] phosphorylate β-tubulin in vitro, but functional and physiological significance of the β-tubulin phosphorylation is not clear. Tubulin phosphorylation precisely at the polymerization interface offers an efficient strategy for reversibly and rapidly regulating microtubule stability in response to biotic and abiotic signals. Because the PHS1-targeted phosphorylation site is highly conserved in almost all eukaryotic α-tubulins, and because the tubulin kinase domain induced microtubule destabilization in animal cells, active PHS1 forms may be used to depolymerize microtubules in cell-type-specific and developmentally controlled manners in various multicellular organisms.

Experimental Procedures

Plant Materials and Growth Conditions

Arabidopsis thaliana seedlings of the Columbia ecotype (Col-0) were grown as described previously [10]. For transient expression assays, *Arabidopsis* seedlings were grown on solid medium containing half-strength Murashige and Skoog (MS) salts, 1% sucrose, 0.05% 2-(N-morpholino)ethanesulfonic acid-potassium hydroxide (MES-KOH) (pH 5.7), 0.05 mg/ml myoinositol, 0.2 μg/ml thiamine, and 0.7% agar for 16–20 days. For stress treatment experiments, 7-day-old *Arabidopsis* seedlings were placed in 5 ml tubes containing 1 ml of distilled water, 0.8 M sorbitol, or 0.4 M NaCl. Time course experiments of osmotic stress used 3-day-old dark-grown seedlings incubated with 1 ml of 0.8 M sorbitol in 5 ml tubes or on slide glass. The T-DNA-tagged null allele *phs1-5* has been described previously [11]. Estradiol (Sigma-Aldrich) stock solution in DMSO was added to a final concentration of 5 μM to the seedlings cultured in liquid half-strength MS medium.

Transient Biolistic Expression Assays

A plasmid (2 μg) harboring PHS1 and the mCherry control plasmid (2 μg) were mixed with 1.5 mg of 1.6 μm gold particles (Bio-Rad) suspended in 19.2% glycerol, 962 mM $CaCl_2$, and 1.5% spermidine and incubated for 30 min at room temperature, washed sequentially with 70% ethyl alcohol (EtOH) and 100% EtOH, and then cobombarded into leaf epidermis cells of 16- to 20-day-old transgenic *Arabidopsis* plants expressing GFP-TUB6 [14] or GFP-fimbrin [31] using the PDS-1000/He Biolistic Particle Delivery System (Bio-Rad) equipped with 1,100 psi rupture disks. After incubation for 12–14 hr in the dark, transfected cells were observed with a D-ECLIPSE C1 confocal microscope (Nikon). A stack of confocal sections (1 μm intervals) across the cell cortex was acquired by excitation at 488 nm for GFP and 544 nm for mCherry. Images were processed using ImageJ 1.47d (http://rsbweb.nih.gov/ij/) and Adobe Photoshop Elements 9.

Microtubule Immunostaining

The microtubules in the root epidermal cells of 4-day-old seedlings were immunostained with rat monoclonal anti-α-tubulin antibody YL1/2 (Abcam) and Alexa Fluor 568 goat anti-rat IgG (Molecular Probes) as described [25]. Fluorescently tagged microtubules were analyzed with a C2 confocal microscope (Nikon). Stacks of images (at 0.275 μm intervals) were taken along the z axis. The methods for microtubule immunostaining in COS-7 cells are shown in Supplemental Experimental Procedures.

Observation of Microtubule Organization under Hyperosmotic Stress

The *UBQ10* promoter-driven GFP-TUB6 construct was stably transformed into WT and *phs1-5 Arabidopsis* plants for this assay. The etiolated hypocotyls of 3-day-old seedlings were incubated in 0.8 M sorbitol on a glass slide at the ambient temperature. Microtubules were analyzed in z stacks of images at 1 μm intervals using a C2 confocal microscope (Nikon).

Protein Extraction and Immunoblotting

Seven-day-old *Arabidopsis* seedlings were frozen in liquid nitrogen, ground in 20 mM sodium phosphate buffer (pH 7.4) containing 100 μM Na_3VO_4, 50 mM β-glycerophosphate, 0.5 mM phenylmethanesulfonylfluoride (PMSF), and Complete Protease Inhibitor Cocktail (Roche). After centrifugation at 10,000 × *g* for 10 min, supernatants were used as crude protein extracts. Protein samples (20 μg each) were separated by SDS-PAGE and blotted onto a polyvinylidene fluoride (PVDF) membrane (Immobilon-P; Merck Millipore). See Supplemental Experimental Procedures for details.

Phos-Tag SDS-PAGE

Phosphorylated proteins were separated on Phos-tag gels according to a published method [18]. Crude protein extracts were precipitated with trichloroacetic acid and dissolved in SDS-PAGE sample buffer to a protein concentration of 1 mg/ml, and 20 μl was loaded on each lane. The SDS-PAGE resolving gel contained 12.5 μM Phos-tag (Wako Pure Chemical), 25 μM $Zn(NO_3)_2$, 357 mM Bis-Tris (pH 6.8), and acrylamide (6% total concentration of acrylamide and bisacrylamide monomer [T], 3.3% bisacrylamide concentration [C]), whereas the running buffer contained 100 mM Tris, 100 mM MOPS, 0.1% SDS, and 5 mM sodium bisulfite. After electrophoresis, gels were washed with 10 mM EDTA in Towbin buffer (25 mM glycine, 192 mM Tris, 10% methanol) for 10 min, with Towbin buffer alone for an additional 10 min, and then used for blotting. The separated proteins were transferred to PVDF membranes (Immobilon-P).

Constructs and Transgenic Plants

All constructs and transgenic plants used in this study are described in Supplemental Experimental Procedures.

Expression and Purification of Recombinant PHS1 Proteins

Recombinant proteins were expressed as fusions to Trigger Factor and Strep tag II (TF-Strep) in the *E. coli* Rosetta strain (Merck Millipore) and purified in Ni-Sepharose resin (GE Healthcare) according to the manufacturer's instructions. The buffer was changed to 50 mM HEPES-KOH (pH 7.5) containing 1 mM dithiothreitol (DTT) using a NAP-5 column (GE Healthcare). After exchanging the buffer, glycerol was added to a final concentration of 30% (v/v), and the protein stock solution was kept at −20°C until use.

In Vitro Phosphorylation Assay

TF-Strep-tagged PHS1 (150 ng) and tubulins (1 μg) were incubated in reaction buffer containing 50 mM HEPES-KOH, 1 mM $MnCl_2$, 1 mM DTT, 50 μM ATP, and 185,000 Bq [γ-^{32}P]ATP for 30 min at 30°C. Tubulins were purified from pig brain [32] or *Arabidopsis* MM2d suspension cultured cells. The reactions were stopped by adding 4× SDS sample buffer. Proteins were

separated on acrylamide gels (7.5% T, 3.3% C) and detected by BAS-3000 (Fujifilm). To separate *Arabidopsis* α-tubulin and β-tubulin, acrylamide gels composed of 7.5% T and 0.66% C were used. The autophosphorylation activity of PHS1 was assayed without tubulins under the same reaction conditions.

Purification of Tubulins and Microtubule-Associated Proteins from *Arabidopsis* Cells and Screening of PHS1 Substrates

Tubulins and microtubule-associated proteins were purified from *Arabidopsis* suspension-cultured cells (MM2d strain) based on a published method for cultured tobacco BY-2 cells [33]. In the purification step to remove vacuoles from protoplasts, the concentration of Percoll (GE Healthcare) in the buffer was 27%, instead of 37% as in the original protocol. The sucrose concentration in the protein extraction buffer was also changed from 15% to 10% in this method. Purified preparations were then applied to anion exchange column chromatography (Resource Q column; GE Healthcare), and separated proteins in each fraction were subjected to a PD-miniTrap G-25 column (GE Healthcare) to exchange the buffer to 50 mM HEPES-KOH (pH 7.5) containing 1 mM DTT. Proteins (15 μl) from each fraction were then used for the in vitro kinase reaction using 150 ng of recombinant PHS1ΔP or PHS1ΔP$^{D309A,\ N324A}$ proteins.

Purification of Tubulins from *Arabidopsis* Plants via TOG Column

Tubulins were affinity purified from *Arabidopsis* plants using an immobilized TOG domain of the XMAP215/Dis1 family protein as reported previously [22]. Briefly, the GST-TOG1/TOG2 protein was expressed in *E. coli* and purified with glutathione Sepharose 4B (GE Healthcare). After dialysis, the recombinant protein was coupled to NHS-activated Sepharose 4 Fast Flow resins (GE Healthcare). Seven-day-old *Arabidopsis* seedlings (14 g) were ground in liquid nitrogen, and proteins were extracted in 80 mM PIPES (pH6.8) containing 1 mM EGTA, 1 mM DTT, Complete Protease Inhibitor Cocktail, 5 mM β-glycerophosphate, 100 μM Na_3VO_4, and 5 mM NaF. Crude protein extracts were cleared by centrifugation (200,000 × *g*, 10 min), and the supernatants were loaded onto the TOG column three times. The loaded column was then washed with 80 mM PIPES (pH 6.8) containing 1 mM EGTA and 100 μM GTP and subjected to the wash/elution/desalt/concentration processes as described previously [22], except that the Tween/glycerol wash step was omitted. Concentrations of the purified tubulin were quantified using Coomassie Protein Assay Reagent (Thermo Scientific) and adjusted to 5–6 μM.

Microtubule Sedimentation Assay In Vitro

In vitro microtubule sedimentation assay was carried out as described previously [26], with slight modifications. Purified tubulins (3.9 μM) were incubated in 80 mM PIPES (pH 6.8), 1 mM EGTA, 1 mM $MgCl_2$, 1 mM guanosine triphosphate (GTP), 5 μM Taxol, and 5% glycerol for 30 min at 30°C. After centrifugation at 72,000 × *g* for 30 min at 30°C, the pellet was suspended in SDS sample buffer. Proteins were separated on 12% SDS-PAGE gels and stained with colloidal Coomassie solution. Gels were scanned, and the intensities of tubulin bands were quantified with Image J 1.44o (http://rsbweb.nih.gov/ij/).

Immunoprecipitation

Immunoprecipitation was performed as described previously [34]. Seven-day-old light-grown seedlings were ground in extraction buffer EB2 (50 mM HEPES-KOH [pH 7.5], 150 mM NaCl, 5 mM EDTA, 5 mM EGTA, 20% glycerol, 5 mM NaF, 100 μM Na_3VO_4, 50 mM β-glycerophosphate, 1 mM DTT, 0.1% Triton X-100, 0.5 mM PMSF, Complete Protease Inhibitor Cocktail). The samples were centrifuged at 21,500 × *g* for 15 min. The protein concentration was adjusted to 1 μg/ml with EB2 buffer. Then, 50 μl of magnetic beads conjugated to GFP antibodies (RQ2; Medical and Biological Laboratories) was added to 400 μl of cell extracts, and the samples were incubated for 30 min at 4°C with gentle rotation. The beads were then washed three times with EB2 and used for the tubulin phosphorylation assay.

Phosphatase Treatment of In Vivo-Phosphorylated Tubulins

Tubulins were immunoprecipitated from sorbitol-treated GFP-TUA6 seedlings as described above. The immunoprecipitated beads were washed with 1 ml of wash buffer (50 mM HEPES-KOH [pH 7.5], 100 mM NaCl, 2 mM $MnCl_2$, 1 mM DTT), resuspended in 100 μl of wash buffer, and divided into three 30 μl aliquots. After the wash buffer was removed, the beads were incubated with or without lambda phosphatase (400 U; NEB) in 100 μl of commercial reaction buffer (NEB) for 5 min at 30°C. Phosphatase inhibitors (5 mM EDTA, 100 μM Na_3VO_4, and 50 mM NaF) were included in one phosphatase-treated sample. Subsequently, the beads were washed once with 50 mM HEPES-KOH (pH 7.5) and 1 mM DTT and suspended in SDS sample buffer.

MS Analysis

Six-day-old seedlings (*phs1-5* and *XVE::PHS1ΔP-GFP/phs1-5*) were treated with 5 μM estradiol for 24 hr in liquid culture and quick frozen with liquid nitrogen. Crude proteins were extracted and immunoprecipitated with the GFP antibody as described above. Pig brain tubulins (1 μg) were phosphorylated by the immunoprecipitated proteins in the reaction buffer (50 mM HEPES-KOH [pH 7.5], 1 mM DTT, 1 mM $MnCl_2$, 50 μM ATP) for 30 min at 30°C, after which reactions were terminated by adding 4× SDS sample buffer. Proteins were separated by 8% SDS-PAGE gels (TEFCO) and stained with Coomassie brilliant blue. Further details are provided in Supplemental Experimental Procedures.

Quantification of Microtubule Density

We analyzed three-dimensional (3D) images of the hypocotyl cells acquired by a C2 confocal microscope (Nikon). The resolution was 0.41, 0.41, and 1.0 μm/voxel along the x, y, and z axis, respectively. The 3D image was converted to a 2D x-y plane image by maximum-intensity projection. The projected image was then filtered by a Gaussian kernel with a SD of 0.5 pixels to reduce noise. Microtubules in the filtered image were enhanced by multiple directional nonmaximum suppression [35]. Pixels with an output signal of 40 or higher were considered to be the microtubule region. Finally, the microtubule regions were converted to one-pixel-thick segments by thinning algorithm [36]. From the segmented image, the length of individual microtubule segment was measured. Microtubule density (*D*) was calculated as

$$D = \frac{\sum_{i=1}^{N} length(S_i)}{A_{ROI}},$$

where S_i is the *i*-th segments, A_{ROI} is the area of region of interest (ROI), and *N* is the total number of the segments. These steps were performed by KbiLineExtract plug-in, and *D* was measured by KbiLineFeature plug-in on ImageJ. These plug-ins are available as part of the KBI ImageJ plug-ins (http://hasezawa.ib.k.u-tokyo.ac.jp/zp/Kbi/ImageJKbiPlugins).

Colocalization Analysis Based on Multichannel Confocal Images

Confocal images of GFP-labeled α-tubulin and mCherry-labeled β-tubulin were analyzed using ImageJ and KBI plug-in package 1192. The maximum-intensity projection was performed to obtain a 2D plane image. For each epidermal cell, a ROI was assigned manually by the "freehand selection tool" of ImageJ. Pearson's correlation coefficients between GFP intensity and mCherry intensity of each pixel in the ROI were calculated by the "bandScatter" command implemented in the plug-in KbiColor.

Supplemental Information

Supplemental Information includes four figures and Supplemental Experimental Procedures and can be found with this article online at http://dx.doi.org/10.1016/j.cub.2013.08.006.

Acknowledgments

We thank Yoshinori Ban and Tsukaho Hattori (Nagoya University) for sharing unpublished information. We are also grateful to Per Widlund (Max Planck Institute for Molecular Cell Biology and Genetics) for the pGEX-6P-1-Stu2 plasmid; Masanori Mishima (Tokyo Metropolitan University) for tubulin images; and Takayuki Kohchi, Ryuichi Nishihama, and Kimitsune Ishizaki (Kyoto University) for providing the *Marchantia* PHS1 sequence. This work was supported partly by grants-in-aid from the Ministry of Education, Science, Sports and Culture of Japan (23012028 and 24114004) and from the Japan Society for the Promotion of Science (JSPS) to T. Hashimoto (23247008), H.N. (2468807), and N.K. (24770038). S.F. was supported by a JSPS Research Fellowship for Young Scientists.

Received: July 4, 2013
Revised: August 2, 2013
Accepted: August 5, 2013
Published: October 10, 2013

References

1. Wasteneys, G.O. (2002). Microtubule organization in the green kingdom: chaos or self-order? J. Cell Sci. *115*, 1345–1354.
2. Bartolini, F., and Gundersen, G.G. (2006). Generation of noncentrosomal microtubule arrays. J. Cell Sci. *119*, 4155–4163.
3. Paredez, A.R., Somerville, C.R., and Ehrhardt, D.W. (2006). Visualization of cellulose synthase demonstrates functional association with microtubules. Science *312*, 1491–1495.
4. Bartolo, M.E., and Carter, J.V. (1991). Microtubules in mesophyll cells of nonacclimated and cold-acclimated spinach : visualization and responses to freezing, low temperature, and dehydration. Plant Physiol. *97*, 175–181.
5. Wang, C., Li, J., and Yuan, M. (2007). Salt tolerance requires cortical microtubule reorganization in *Arabidopsis*. Plant Cell Physiol. *48*, 1534–1547.
6. Hussey, P.J., and Hashimoto, T. (2009). The cytoskeleton and signal transduction: Role and regulation of plant actin- and microtubule-binding proteins. In Annual Plant Reviews, Volume 33: Intracellular Signaling in Plants, Z. Yang, ed. (Oxford: Wiley-Blackwell), pp. 244–272.
7. Nick, P. (2008). Microtubules as sensors for abiotic stimuli. In Plant Microtubules, P. Nick, ed. (Berlin: Springer-Verlag), pp. 175–203.
8. Hardham, A.R. (2013). Microtubules and biotic interactions. Plant J. *75*, 278–289.
9. De Storme, N., Copenhaver, G.P., and Geelen, D. (2012). Production of diploid male gametes in *Arabidopsis* by cold-induced destabilization of postmeiotic radial microtubule arrays. Plant Physiol. *160*, 1808–1826.
10. Naoi, K., and Hashimoto, T. (2004). A semidominant mutation in an *Arabidopsis* mitogen-activated protein kinase phosphatase-like gene compromises cortical microtubule organization. Plant Cell *16*, 1841–1853.
11. Pytela, J., Kato, T., and Hashimoto, T. (2010). Mitogen-activated protein kinase phosphatase PHS1 is retained in the cytoplasm by nuclear extrusion signal-dependent and independent mechanisms. Planta *231*, 1311–1322.
12. Walia, A., Lee, J.S., Wasteneys, G., and Ellis, B. (2009). *Arabidopsis* mitogen-activated protein kinase MPK18 mediates cortical microtubule functions in plant cells. Plant J. *59*, 565–575.
13. Andreasson, E., and Ellis, B. (2010). Convergence and specificity in the *Arabidopsis* MAPK nexus. Trends Plant Sci. *15*, 106–113.
14. Nakamura, M., Naoi, K., Shoji, T., and Hashimoto, T. (2004). Low concentrations of propyzamide and oryzalin alter microtubule dynamics in *Arabidopsis* epidermal cells. Plant Cell Physiol. *45*, 1330–1334.
15. Gettemans, J., De Ville, Y., Vandekerckhove, J., and Waelkens, E. (1992). Physarum actin is phosphorylated as the actin-fragmin complex at residues Thr203 and Thr202 by a specific 80 kDa kinase. EMBO J. *11*, 3185–3191.
16. Eichinger, L., Bomblies, L., Vandekerckhove, J., Schleicher, M., and Gettemans, J. (1996). A novel type of protein kinase phosphorylates actin in the actin-fragmin complex. EMBO J. *15*, 5547–5556.
17. Steinbacher, S., Hof, P., Eichinger, L., Schleicher, M., Gettemans, J., Vandekerckhove, J., Huber, R., and Benz, J. (1999). The crystal structure of the Physarum polycephalum actin-fragmin kinase: an atypical protein kinase with a specialized substrate-binding domain. EMBO J. *18*, 2923–2929.
18. Kinoshita, E., and Kinoshita-Kikuta, E. (2011). Improved Phos-tag SDS-PAGE under neutral pH conditions for advanced protein phosphorylation profiling. Proteomics *11*, 319–323.
19. Sugiyama, N., Nakagami, H., Mochida, K., Daudi, A., Tomita, M., Shirasu, K., and Ishihama, Y. (2008). Large-scale phosphorylation mapping reveals the extent of tyrosine phosphorylation in *Arabidopsis*. Mol. Syst. Biol. *4*, 193.
20. Wang, X., Bian, Y., Cheng, K., Gu, L.F., Ye, M., Zou, H., Sun, S.S., and He, J.X. (2013). A large-scale protein phosphorylation analysis reveals novel phosphorylation motifs and phosphoregulatory networks in *Arabidopsis*. J. Proteomics *78*, 486–498.
21. Nogales, E., Whittaker, M., Milligan, R.A., and Downing, K.H. (1999). High-resolution model of the microtubule. Cell *96*, 79–88.
22. Widlund, P.O., Podolski, M., Reber, S., Alper, J., Storch, M., Hyman, A.A., Howard, J., and Drechsel, D.N. (2012). One-step purification of assembly-competent tubulin from diverse eukaryotic sources. Mol. Biol. Cell *23*, 4393–4401.
23. Shoji, T., Suzuki, K., Abe, T., Kaneko, Y., Shi, H., Zhu, J.K., Rus, A., Hasegawa, P.M., and Hashimoto, T. (2006). Salt stress affects cortical microtubule organization and helical growth in *Arabidopsis*. Plant Cell Physiol. *47*, 1158–1168.
24. Ban, Y., Kobayashi, Y., Hara, T., Hamada, T., Hashimoto, T., Takeda, S., and Hattori, T. (2013). α-tubulin is rapidly phosphorylated in response to hyperosmotic stress in rice and *Arabidopsis*. Plant Cell Physiol. *54*, 848–858.
25. Ishida, T., Kaneko, Y., Iwano, M., and Hashimoto, T. (2007). Helical microtubule arrays in a collection of twisting tubulin mutants of *Arabidopsis thaliana*. Proc. Natl. Acad. Sci. USA *104*, 8544–8549.
26. Johnson, V., Ayaz, P., Huddleston, P., and Rice, L.M. (2011). Design, overexpression, and purification of polymerization-blocked yeast $\alpha\beta$-tubulin mutants. Biochemistry *50*, 8636–8644.
27. Wloga, D., and Gaertig, J. (2010). Post-translational modifications of microtubules. J. Cell Sci. *123*, 3447–3455.
28. Janke, C., and Bulinski, J.C. (2011). Post-translational regulation of the microtubule cytoskeleton: mechanisms and functions. Nat. Rev. Mol. Cell Biol. *12*, 773–786.
29. Ben-Nissan, G., Cui, W., Kim, D.J., Yang, Y., Yoo, B.C., and Lee, J.Y. (2008). *Arabidopsis* casein kinase 1-like 6 contains a microtubule-binding domain and affects the organization of cortical microtubules. Plant Physiol. *148*, 1897–1907.
30. Motose, H., Hamada, T., Yoshimoto, K., Murata, T., Hasebe, M., Watanabe, Y., Hashimoto, T., Sakai, T., and Takahashi, T. (2011). NIMA-related kinases 6, 4, and 5 interact with each other to regulate microtubule organization during epidermal cell expansion in *Arabidopsis thaliana*. Plant J. *67*, 993–1005.
31. Sheahan, M.B., Staiger, C.J., Rose, R.J., and McCurdy, D.W. (2004). A green fluorescent protein fusion to actin-binding domain 2 of *Arabidopsis* fimbrin highlights new features of a dynamic actin cytoskeleton in live plant cells. Plant Physiol. *136*, 3968–3978.
32. Itoh, T.J., Hisanaga, S., Hosoi, T., Kishimoto, T., and Hotani, H. (1997). Phosphorylation states of microtubule-associated protein 2 (MAP2) determine the regulatory role of MAP2 in microtubule dynamics. Biochemistry *36*, 12574–12582.
33. Hamada, T., Igarashi, H., Itoh, T.J., Shimmen, T., and Sonobe, S. (2004). Characterization of a 200 kDa microtubule-associated protein of tobacco BY-2 cells, a member of the XMAP215/MOR1 family. Plant Cell Physiol. *45*, 1233–1242.
34. Takahashi, F., Mizoguchi, T., Yoshida, R., Ichimura, K., and Shinozaki, K. (2011). Calmodulin-dependent activation of MAP kinase for ROS homeostasis in Arabidopsis. Mol. Cell *41*, 649–660.
35. Sun, C., and Vallotton, P. (2009). Fast linear feature detection using multiple directional non-maximum suppression. J. Microsc. *234*, 147–157.
36. Wu, R.-Y., and Tsai, W.-H. (1992). A new one-pass parallel thinning algorithm for binary images. Pattern Recognit. Lett. *13*, 715–723.